Dalton Transactions

ROYAL SOCIETY OF CHEMISTRY

PERSPECTIVE

View Article Online
View Journal | View Issue

Cite this: *Dalton Trans.*, 2026, **55**, 563

Recent advances in one-dimensional tubular composites with MoO_3-based micro/nanorods as templates

Xiaohong Xu, Min Zhang, * Jingli Xu and Xue-Bo Yin *

Received 27th September 2025,
Accepted 7th November 2025

DOI: 10.1039/d5dt02309b

rsc.li/dalton

Template-mediated strategies are a versatile and scalable approach for fabricating one-dimensional (1D) tubular composites, while molybdenum trioxide (MoO_3) micro/nanorods have emerged as promising templates for engineering hollow nanostructures. In this minireview, we systematically introduce recent advancements in a series of MoO_3-based micro/nanorods for guiding the formation of 1D tubular composites with different structural characteristics. We summarize the various rational design strategies, such as hard-templating and self-templating methodologies, as well as derivative strategies with organic polymer coating and functional oxide coating for MoO_3-derived 1D tubular composites. Notably, the architectures, structures, compositions, and morphologies of these composites are discussed for their applications in catalysis, protein adsorption, and enzyme-mimic reactions, among others. Finally, we critically evaluate the prospects, challenges, and opportunities for advancing MoO_3-derived 1D tubular nanostructures toward next-generation nanocatalytic and environmental remediation technologies.

1. Introduction

One-dimensional (1D) hollow composites have attracted significant attention due to their high specific surface area, unique structures, and exposed active sites. The high specific surface area enhances mass transport, and the exposed active sites improve substrate accessibility. Thus, 1D hollow composites exhibit extensive applications with improved performance as a promising matrix for energy storage, catalysis, adsorption and sensing. However, direct preparation often shows low efficiency and yield. As an alternative, the template-engineering strategy especially becomes powerful and efficient for the preparation of 1D hollow composites. Thus, some materials with micro/nanorod structures are first prepared and then used as templates to guide the assembly of functional materials. According to special applications, the templates can be removed or retained. Therefore, the templates should be easily prepared as micro/nanorod structures and removed.

MoO_3 is easily prepared as a unique 1D micro/nanorod structure and shows great potential as a template for the fabrication of 1D hollow nanostructures.[1,2] However, the evolutionary pathway of MoO_3-templated synthesis underscores the continuous refinement of its one-dimensional morphology. Hard-templating strategies have often been hindered by two major challenges: the incomplete removal of the MoO_3 core and the consequent structural collapse of the deposited shell. These limitations have motivated the shift toward self-templating approaches, which utilize *in situ* chemical transformation of MoO_3 precursors to entirely circumvent the etching step and enable the synthesis of Mo-based derivative materials. Nevertheless, structural collapse and aggregation during conversion remain challenges. A pivotal advancement addressed this through surface engineering, where pre-formed rigid overlayers (*e.g.*, polymers or covalent organic frameworks) act as structural scaffolds. These supports preserve the rod-like morphology throughout the transformation, thereby facilitating a strategic transition from mere morphological replication to synergistic structure and composition design.[3–12]

MoO_3 micro/nanorods possess a layered structure and multiple valence states with abundant interactions as versatile templates for the integration of functional materials to obtain 1D hollow nanomaterials. Additionally, their high aspect ratio and stability enhance flexibility and accessibility for creating hollow structures with controllable dimensions and morphologies. Moreover, MoO_3 micro/nanorods are easily prepared in large quantities using simple hydrothermal or sol–gel strategies, making them cost-effective for the industrial-scale production of tubular nanostructures.[13,14] These attributes collectively position MoO_3 micro/nanorods as a versatile template for the rational design of hollow nanomaterials with tailored functionalities to improve the performance of integrated functional materials. Thus, the MoO_3 micro/nanorod-based template strategy offers several distinct advantages for

College of Chemistry and Chemical Engineering, Shanghai University of Engineering Science, Shanghai 201620, China. E-mail: zhangmin@sues.edu.cn, xbyin@nankai.edu.cn

engineering 1D hollow nanomaterials: (1) anisotropic morphology control: the inherent 1D rod-like structure of MoO_3 enables the as-prepared hollow nanotubes with high aspect ratios and uniform diameters, being critical for applications with directional mass/electron transport (*e.g.*, catalysis and energy storage). (2) Facile template removal: the MoO_3 template can be selectively etched with mild basic solutions, leading to the formation of hollow architectures without residual template fragments. (3) Self-templating capability: MoO_3 is easily transferred to MoS_2, $NiMoO_4$, and MoO_2 through phase transformations after sulfidation, nickel-mediated hydrothermal reaction or reduction conditions, while the 1D micro-/nanostructures are retained. Thus, a series of MoO_3-based template materials are selected for improved performance. (4) Surface reactivity: the layered MoO_3 structure facilitates the conformal coating of polymers (*e.g.*, PPy), carbon, or metal oxides, enabling precise control over shell thickness and composition. In addition to the aforementioned advantages, MoO_3 templates also offer the following several benefits compared to traditional templates like nanorods, SiO_2, carbon nanotubes, and metal oxide templates: (1) inherent 1D morphology: MoO_3 naturally forms layered orthorhombic structures that easily grow into nanorods without the need for shape-directing agents. This makes its synthesis far simpler than that relying on CNTs or SiO_2 templates. (2) Tunable architecture: the interlayer spacing of MoO_3 enables ion/molecule intercalation. This capability enables precise regulation of wall thickness and porosity, which is a feature not achievable with carbon nanotubes or metal oxide templates. (3) Intrinsic surface reactivity: owing to its Lewis acidic and redox-active surface, MoO_3 allows for direct polymerization or deposition of functional coatings. By comparison, inert templates, like CNTs or SiO_2, often require pre-functionalization.[15–20] Thus, a series of MoO_3-based micro/nanorods can be selected as templates to tune the composites, structures, and performance of 1D hollow nanomaterials. In combination with charge distribution, active site availability, structural design, morphological control, and surface functionalization, significant breakthroughs are expected in the activity, selectivity, and stability of various applications, as illustrated in Fig. 1.

The central focus of this minireview is to illustrate the intricate correlations of MoO_3 1D tubular composite's structural parameters, compositional features and functional applications. By evaluating these structure–function relationships, we provide targeted optimization for specific catalytic reactions and adsorption processes. Finally, we propose a forward-looking perspective on integrating tubular nanostructures with multifunctional components to create adaptive platforms for enzyme-mimic reactions, adsorption capacities and energy storage.

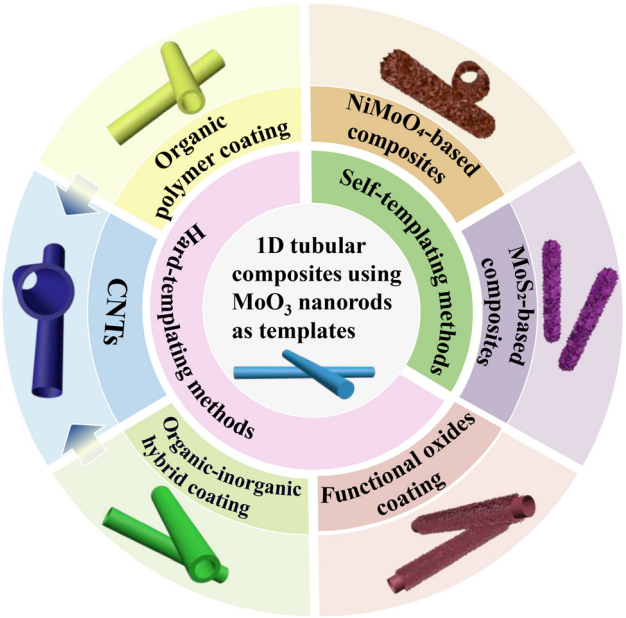

Fig. 1 The preparation of 1D tubular composites using MoO_3 micro/nanorods as templates. MoO_3-based micro/nanorods are used for the preparation of 1D tubular composites with hard-templating and self-templating strategies with polymers, organic–inorganic species, CNTs, oxides and others as the matrices. The functions and merits of tubular materials are integrated.

2. Hard templating

2.1 Design and synthesis of a hard-templating strategy

The hard templating method presents a conceptually straightforward strategy for synthesizing hollow nanostructures.[21] The hard templating process involves three sequential steps: (1) synthesis of MoO_3 templates with tailored shapes; (2) conformal coating/deposition of target materials *via* sol–gel chemistry, hydrothermal reactions, or electrochemical methods; and (3) selective removal of the MoO_3 core through chemical etching or thermal decomposition to yield hollow tubules.[22,23] Although the MoO_3 template did not constitute the final elemental composition of the material, it determined the final nanotube structure. Han *et al.* successfully synthesized a precisely structured tubular architecture composed of carbon-coated Fe_3O_4, characterized by a hierarchically porous design.[24] An efficient two-step method was developed by Hu *et al.* to synthesize hierarchical MoO_3/SnS_2 core–shell nanocables, where ultrathin SnS_2 nanosheets are vertically grown on MoO_3 nanobelts to form a heterointerface.[25] Yuan *et al.* fabricated hierarchical hollow FeCo-LDH@CoSx microtubes by sequentially depositing FeCo-LDH and ZIF-67 onto MoO_3 microrod templates, with subsequent sulfidation and template etching.[26]

2.2 One-dimensional N-doped carbon nanotubes (NCNTs)

NCNTs have the advantage of high specific surface area, exceptional chemical stability, porous structure and rapid electron transfer kinetics.[27–32] The distinctive characteristic of NCNTs renders them an indispensable material for cutting-edge applications in advanced electrocatalysis, energy storage, and sensing technologies. By further enhancing the binding interactions between NCNTs and catalytic species, we can improve catalytic performance.[33–37]

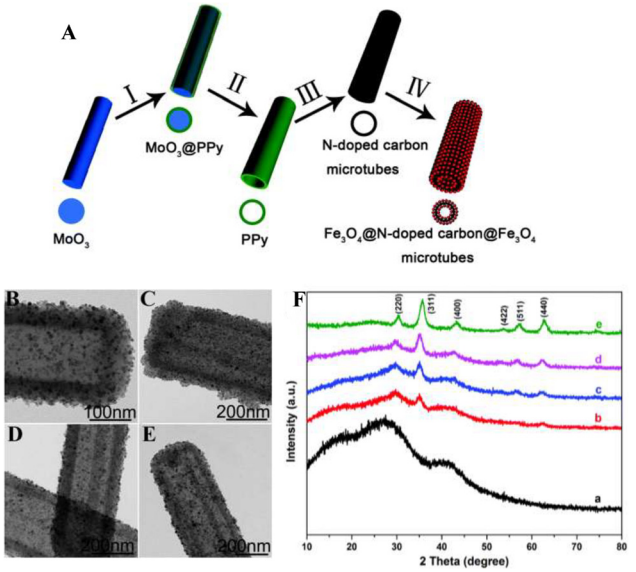

Fig. 2 (A) Schematic of the formation of the Fe_3O_4@N-doped carbon@Fe_3O_4 microtubes using a multi-step conversion route. (B–E) TEM images of the Fe_3O_4@N-doped carbon@Fe_3O_4 microtubes upon increasing the weight ratio between $Fe(acac)_3$ and the N-doped carbon microtubes from 0.5 : 1; 2 : 1; 4 : 1; and 10 : 1. (F) the X-ray diffraction patterns of the N-doped carbon microtubes (a) and Fe_3O_4@N-doped carbon@Fe_3O_4 microtubes using different ratios of $Fe(acac)_3$ to N-doped carbon microtubes: (b) 1 : 2, (c) 2 : 1, (d) 4 : 1 and (e) 10 : 1.

Our group designed a series of hierarchical NCNT architectures. For instance, Zhang *et al.* fabricated triple-walled M@N-doped carbon @M microtubes (M = Fe_3O_4, Cu/Cu_2O, MnO_2, and MoS_2), as shown in Fig. 2. Initially, they employed a one-pot oxidative polymerization approach to synthesize MoO_3@PPy composites. Subsequently, Fe_3O_4 NPs were uniformly distributed and deposited on both the internal and external surfaces of the NCNTs *via* a high-temperature thermal decomposition process.[38,39] Additionally, the PPy shell exhibits the capability to adsorb Fe^{3+} ions, which is attributed to the robust coordination interactions occurring between Fe^{3+} ions and the nitrogen atoms within the PPy structure.[40] For example, Fe_3O_4@NCMTs demonstrate structural superiority, and this superiority could potentially arise from void-confinement effects as well as optimized substrate access and electron transfer.[41] The C@Fe_3O_4@C/Ni structure has the potential to enhance the dispersion and surface accessibility of Ni NPs. Notably, its inner and outermost nitrogen-doped porous graphitic carbon layers work in a synergistic manner. This structure not only improves mass transport kinetics and electronic conductivity but also offers robust protection to the Fe_3O_4 and Ni NPs.[42] Furthermore, based on our previous studies, we accomplished precise control over the hierarchical porosity of 1D magnetic metal silicate microtubes.[43–45] Recently, Miao *et al.* conducted NCMTs@Fe_3O_4@SiO_2@C/Ni–Co–Cu,[46] and Zheng *et al.* developed a biosensing platform utilizing NCMTs@Fe_3O_4@Cusilicate, which achieves the ultrasensitive detection of carcinoembryonic antigen (CEA).[47,48] These composite materials contain uniformly dispersed metallic NPs embedded within carbon layers. Due to their hierarchical architecture, large specific surface area, and high metal nanoparticle density, these materials exhibit exceptional catalytic performance.

2.3 Organic–inorganic hybrid coating methods

MoO_3 micro/nanorods were coated with three distinct polymeric layers: organic polymers, metal–organic polymers, and inorganic–organic hybrid polymers. Organic polymer coatings effectively stabilize MoO_3's unique 1D tubular structure, endow its surfaces with redox-active groups, and markedly enhance its electrical conductivity.[49–52] Subsequently, the MoO_3 cores underwent selective removal through thermal decomposition or etching processes. This operation enabled the successful construction of core–shell structures.[53–57] These hollow nanocomposites exhibit significantly larger surface areas, readily accessible active sites, and a diverse array of multiple functions. Owing to these characteristics, they demonstrate exceptional suitability for applications in catalysis, energy storage, and environmental remediation.[58–63]

During our research, we successfully developed certain composites with organic–inorganic hybrid coatings, utilizing MoO_3 microrods as sacrificial templates. Through subsequent coating of PPy and the PDA-Ni^{2+} complex in an ammonia solution, PPy@PDA-Ni^{2+} microtubes were successfully synthesized. Following an annealing treatment, these microtubes were transformed into Ni NP-anchored N-doped carbon microtubes, which exhibited excellent performance in 4-NP reduction.[64]

2.4 Functional oxide coating methods

The functional oxide coating strategy has the advantage of a hierarchically porous structure, extremely high specific surface area, hierarchical porosity, multi-component interfaces, and optimally adjusted carbon coating thickness. These features make it promising for applications in advanced nanocomposites, including energy conversion, catalysis, and sensing.[65–70] MoO_3 microrods also served as sacrificial templates, and FeOOH and PDA-Ni^{2+} served as Fe_3O_4 and C/Ni precursors, respectively. PDA-Ni^{2+} was polymerized on MoO_3@FeOOH core using an extended Stöber method, and ammonia-mediated etching removed the MoO_3 template and stabilized the PDA-Ni^{2+} coating at the same time.[71] In another study, NiCo-LDH NSs were vertically grown on the MoO_3@FeOOH nanorods using a urea-assisted co-precipitation method, resulting in the formation of a hierarchical dual-layer architecture.[72] After alkaline etching, the MoO_3 cores were dissolved, leaving hollow structures with FeOOH/NiCo-LDH shells.[73] The FeOOH intermediate not only enhances the adhesion between the MoO_3 template and the NiCo-LDH overlayer but also incorporates redox-active Fe into the overall structure. Simultaneously, the NiCo-LDH overlayer provides an abundant array of catalytic sites and establishes efficient ion-transport pathways. Subsequently, the MoO_3@FeOOH and MoO_3@NiCo-LDH nanorods were further modified with SiO_2 and PDA. MoO_3 microrods served as

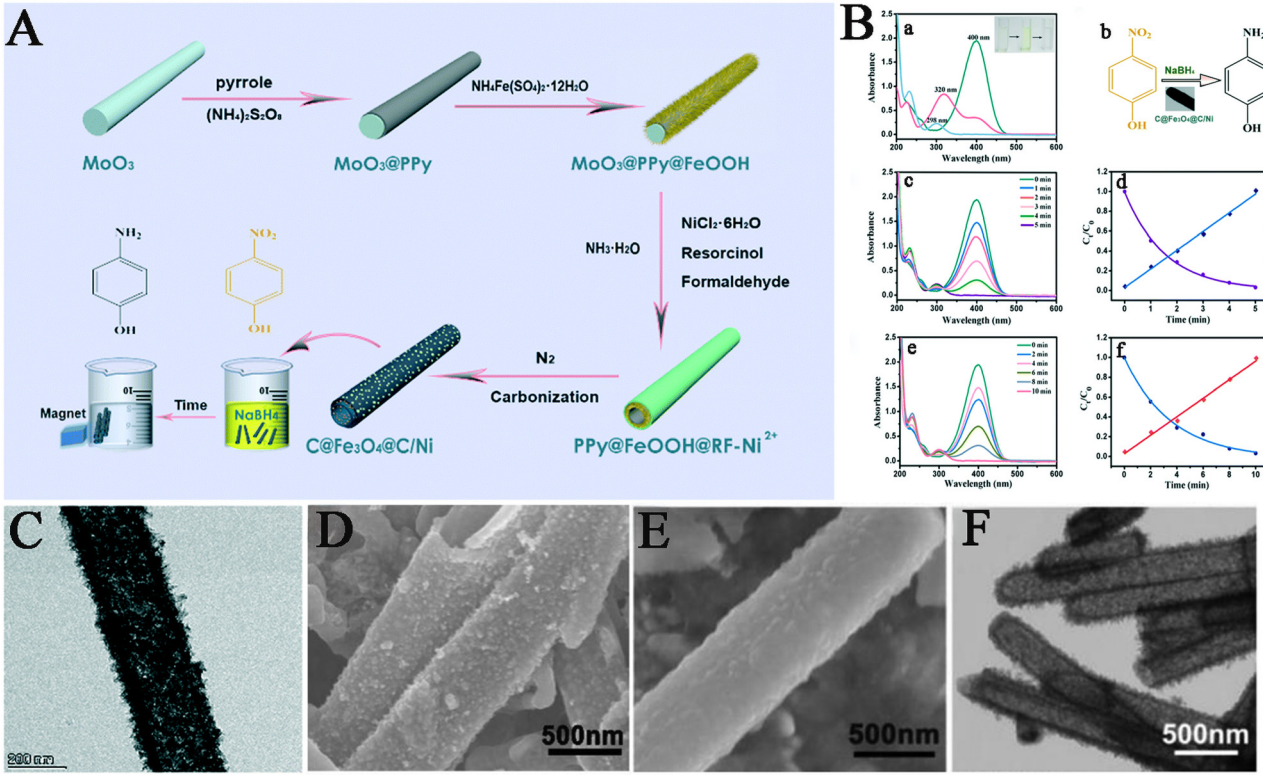

Fig. 3 (A) A schematic of the fabrication procedures of the sandwich-like C@Fe_3O_4@C/Ni microtubes; (B) the UV-vis absorption spectra evaluate the catalytic ability of the as-prepared C@Fe_3O_4@C/Ni microtubes: (a and b) illustration of the 4-NP reduction; (c) successive reduction of 4-NP using C@Fe_3O_4@C/Ni-500 as a catalyst; (d) C_t/C_0 and $\ln(C_t/C_0)$ *versus* reaction time for the reduction of 4-NP over C@Fe_3O_4@C/Ni-500; (e) successive reduction of 4-NP using C@Fe_3O_4@C/Ni-700 as a catalyst; and (f) C_t/C_0 and $\ln(C_t/C_0)$ *versus* reaction time for the reduction of 4-NP over C@Fe_3O_4@C/Ni-700; SEM and TEM images of C@Fe_3O_4@C/Ni-500 (C and D) and PPy@FeOOH@RF-Ni^{2+}(E and F).

sacrificial templates, and the extended Stöber method achieved the sequential deposition of SiO_2 and PDA-Ni^{2+} layers and enhanced the dispersibility and density of the Ni nanoparticles. As shown in Fig. 3, the Fe_3O_4@SiO_2@C/Ni nanocomposite demonstrated exceptional catalytic performance in 4-NP and exhibited remarkably selective adsorption capabilities toward His-rich proteins. The test results demonstrate that the superior catalytic performance and stability of the material originate from its well-defined porous structure, abundant active sites, and strong magnetic properties.[74]

3. Self-templating strategy

3.1 Design and synthesis of self-templating

Unlike hard-templating methods, self-templating synthesis guides the formation of the nanostructure's shape and contributes to the final material composition. From a synthetic perspective, MoO_3 templates are transformed into hierarchical hollow tubular frameworks composed of Mo-based compounds.[75–77]

Kim *et al.* reported an innovative approach, employing a two-step hydrothermal synthesis technique to successfully achieve a morphological transformation from MoO_3 nanorods to $NiMoO_4$ nanotubes.[78] A self-templating approach was employed by Adhikari *et al.* to fabricate hollow nanostructured molybdenum trioxide encapsulated within a PPy shell.[79] Furthermore, Tang *et al.* synthesized a novel MoS_2/SnS@C hollow nanotube using a straightforward solvothermal approach. They found that this unique hollow nanotube not only reinforces the structural stability of the material but also offers an efficient and spacious pathway for facilitating sodium-ion migration.[80] Chen *et al.* proposed a metal-cation-directed self-assembly method to fabricate hierarchical hollow MoS_2 nanotubes. Metal cations induce substantial 1T-phase MoS_2 formation, offering a practical way to create high-1T-content hollow MoS_2 nanostructures.[81] Wang *et al.* utilized FeOOH/$NiMoO_4$@PDA as precursors, and NCMTs were embedded with $FeNi_3$ and MoO_2 NPs. The NCMTs@MoO_2/$FeNi_3$ composite displays outstanding uniformity and possesses a well-defined hierarchical hollow architecture.[82] The synthesis of $NiMoO_4$@FeOOH/$NiMoO_4$@$NiMoO_4$ and FeOOH/(NiCo)MoO_4 demonstrates the effectiveness of combining structural design, electronic tuning, and computational modeling. This multi-method approach enhances electrochemical performance and material stability, highlighting its potential for advanced energy technologies.[83,84] He *et al.* successfully developed hierarchical TiO_2@MoS_2 hollow microtubes through

a combination of hydrothermal, sol–gel, and sulfidation processes. TiO_2 served as an excellent solid support, significantly inhibiting the aggregation of MoS_2 NSs. Notably, sulfidation hydrothermal treatment converts the amorphous phase of TiO_2 microtubes into mesoporous anatase TiO_2 microtubes. This hollow architecture exhibits synergistic integration, with interfacial adsorption effects occurring between MoS_2 NSs and mesoporous TiO_2. Through experimental data, the TiO_2@MoS_2 microtubes show the highest removal efficiency (81.31%) for aqueous RhB, significantly outperforming pure TiO_2 microtubes (3.90%) or pure MoS_2 nanosheets (43.77%). This enhancement stems from the synergistic interaction between TiO_2 and MoS_2, which boosts photocatalytic degradation. The findings offer insights for designing efficient photocatalysts for pollutant removal.[85]

Decorating organic molecules and organic–inorganic molecules *via* a polymer-confined sulfidation strategy on the surface of MoS_2 can improve the performance.[86] We developed a hydrothermal method to yield a series of tubular MoS_2-based nanocomposites based on MoO_3@PANI/PPy/APTES/COF microcables.[87–90] Decorating MoS_2 NSs with organic matrices has exhibited markedly enhanced performance in sensing, photoelectron catalysis, energy storage, and lubrication.[91–93] As a representative of organic conductive polymers, PANI demonstrates outstanding structural stability.[94,95] Li *et al.* successfully synthesized hierarchical PANI microtubes, which were subsequently enveloped by MoS_2 NSs to form a core–shell heterostructure. Then, the outer MoS_2 shell underwent further modification by being doped with Fe_3O_4 NPs and noble metal NPs. This meticulous modification facilitated the establishment of a highly versatile multifunctional heterostructure interface, exhibiting synergistic properties for advanced applications.[96] In another study, through a dissolution-regrowth mechanism, the MoO_3@PPy microtubes were transformed into hollow PPy@MoS_2 sheet-like nanostructures.[97] This architecture offers dual advantages: (1) the sheet-like morphology of MoS_2 significantly enhances electrical conductivity while effectively minimizing the agglomeration of nanosheets. (2) The conductive PPy core serves as a facilitator for the *in situ* reduction and uniform dispersion of Ag, Au, or Pd NPs on the MoS_2 surface, as shown in Fig. 4. For example, MoO_3@FeOOH as a precursor enables the targeted and selective deposition of Fe-doped MoS_2 nanosheets onto conductive PPy microtubes.[98]

Leveraging this platform, as shown in Fig. 5, Lu *et al.* developed programmable metal-nanoparticle-supported nanozymes (MNNs) on PPy@MoS_2 matrices. These metal NPs can modulate the catalytic properties of PPy@MoS_2 nanocomposites, enabling them to act as an ideal alternative to DNA-AuNP conjugates in sensor arrays. The sensor array demonstrated outstanding discriminatory capability, even when subjected to analysis within the highly complex matrix of physiological fluids. This exceptional performance enabled precise and accurate differentiation among blind samples, serum proteins, heat-denatured proteins, and clinical cancer biomarkers.[99]

Besides, APTES establishes covalent linkages with the MoO_3 surface *via* its –Si–OH functional group. This covalent interaction augments the intrinsic properties of the resulting nanocomposites and significantly enhances their dispersion stability when suspended in polar solvents.[100] Using MoO_3 microrods as self-sacrificial templates, we crafted a tubular structure through an APTES-modified synthesis, yielding a precisely structured APTES@MoS_2 tubular composite.[101] Furthermore, by finely adjusting the interfacial interactions at the COF/MoS_2 heterojunction, we can strategically optimize the reaction pathways, thereby enhancing the catalytic performance.[102,103] Guo *et al.* fabricated hierarchical COFs@MoS_2-Pd hybrid architectures, wherein the vertically oriented MoS_2 NSs provide a wealth of active sites and facilitate the dense and uniform distribution of Pd NPs, which exhibited excellent performance in the reduction of 4-NP and enzyme-like catalysis.[104]

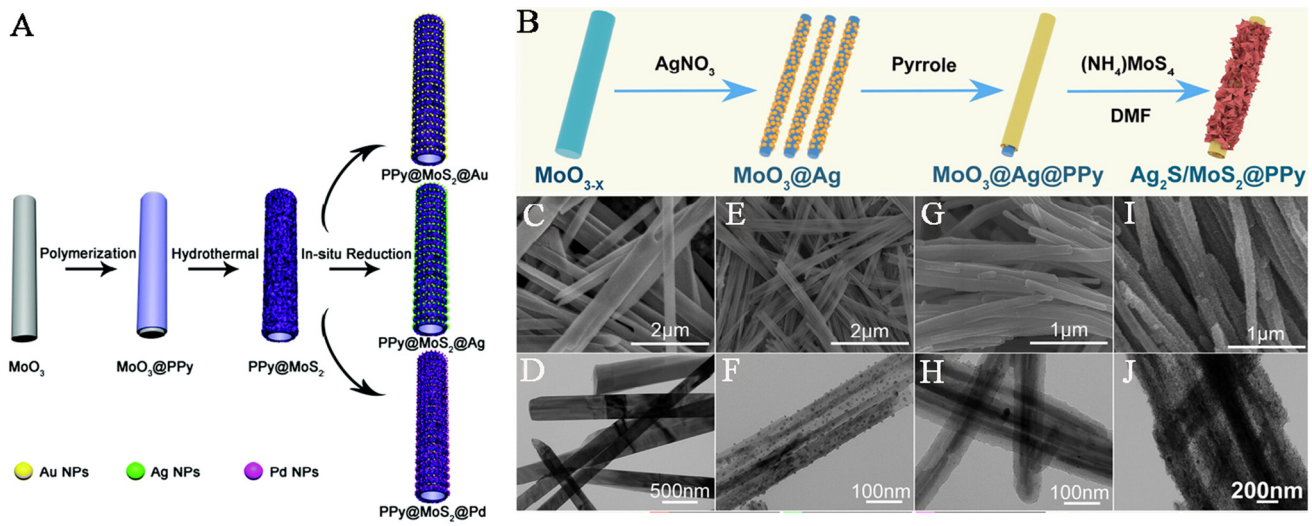

Fig. 4 (A) Schematic synthesis of PPy@MoS_2@Au/Ag/Pd composites. (B) Schematic of the synthetic procedure of Ag_2S/MoS_2@PPy nanotubes. SEM and TEM images of (C and D) MoO_{3-x}, (E and F) MoO_3@Ag nanorods, (G and H) MoO_3@Ag@PPy nanorods, and (I and J) Ag_2S/MoS_2@PPy nanotubes.

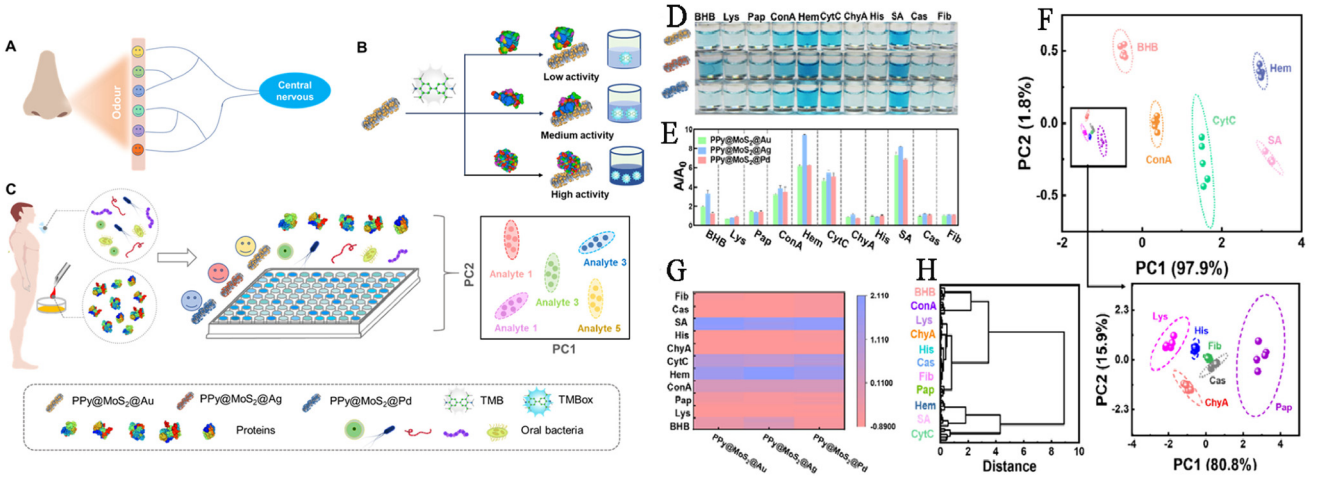

Fig. 5 (A) Working principle of the mammalian olfactory system; (B) modulation of the catalytic oxidation of metal-NP-supported nanozyme (MNN) by different proteins; (C) colorimetric sensor arrays for pattern recognition of proteins and oral bacteria based on the MNNs; (D) color change patterns of TMB oxidation catalyzed by the MNN sensor array in the presence of different proteins; and (E) colorimetric response patterns (A/A_0) at 652 nm against different proteins. The error bar shows the standard deviation of five independent measurements. (F) Canonical score plots for the first two factors of colorimetric response patterns obtained from PCA with 95% confidence ellipses (n = 5). (G) Heat map derived from colorimetric response patterns for 11 proteins. (H) Hierarchical cluster analysis (HCA) plot for the discrimination of 11 proteins. The concentration of each protein was 250 nM.

4. Conclusion and outlook

This minireview summarizes recent advances for 1D tubular composites with MoO_3-based micro/nanorods as templates. The integration of MoO_3-derived templates with functional components, including carbonaceous matrices, metal oxides, and conductive polymers, yields a variety of tubular nanocomposites. These nanocomposites exhibit distinct structural advantages and superior electronic/catalytic properties. Despite having achieved significant progress in template-directed synthesis, 1D hollow nanostructures continue to face critical challenges using MoO_3-based micro/nanorods as templates. Looking ahead, several promising research directions are poised to shape the future of this field. First, there is a growing impetus toward the design of multi-component and multi-shelled hollow structures. Future work will likely focus on the sequential deposition of more than two functional layers (*e.g.*, ternary metal sulfides and their hybrids with conductive polymers) onto the MoO_3 template, creating complex tubular structures with intimately coupled interfaces for enhanced synergistic effects. Second, the precision control over the microstructure of the deposited shells represents a critical frontier. Moving beyond simple coating, strategies to engineer defects, crystallinity, and porosity at the atomic or nanoscale within the shell walls will be crucial for maximizing the density and accessibility of active sites. This includes developing milder etching processes that preserve the integrity of these delicate nanostructures. Third, expanding the functional repertoire of these materials beyond electrocatalysis and energy storage is a key trend. Their application in areas such as sensors, nanoreactors, and biomedical devices (*e.g.*, for drug delivery or theranostics) remains largely unexplored. Finally, bridging the gap between fundamental studies and practical applications requires a stronger emphasis on scalability and stability. Future efforts must address the challenges of large-scale, reproducible synthesis and rigorously evaluate the long-term operational stability of these 1D hollow composites under harsh conditions. In conclusion, the future of MoO_3-templated 1D hollow nanomaterials lies in moving from structural complexity to functional intelligibility, paving the way for their deployment in next-generation technologies.

Conflicts of interest

The authors declare no competing financial interest.

Data availability

This review paper does not contain original data. All the figures were cited from the literature after permission.

Acknowledgements

This study was supported by the National Natural Science Foundation of China (Grants 22374096 and 22174077) and the Class III Peak Discipline of Shanghai-Materials Science and Engineering (High-Energy Beam Intelligent Processing and Green Manufacturing).

References

1 D. V. Pham, R. A. Patil, C. C. Yang, W. C. Yeh and Y. Liou, *Nano Energy*, 2018, **47**, 105–114.
2 J. Zhao, J. Xu, X. B. Yin and M. Zhang, *Cryst. Growth Des.*, 2025, **25**(19), 8172–8180.
3 W. Tian, H. Hu, Y. Wang, P. Li and J. Liu, *ACS Nano*, 2018, **12**(2), 1990–2000.
4 M. Kawase, K. Akaike, K. Aoyama, Y. Ito, M. Tamura and K. Kanai, *Appl. Catal., B*, 2020, **273**, 119068.
5 B. Mandal, M. Das, M. T. Htay and S. Mukherjee, *Mater. Res. Bull.*, 2019, **109**, 281–290.
6 R. S. Kangutkar, P. Walko, P. L. Dhepe, G. P. Nayaka and J. Manjanna, *ACS Appl. Nano Mater.*, 2025, **8**(14), 7175–7189.
7 M. Cheng, P. Lv, X. Zhang, Z. Guo, Z. Wang, Z. Zhou and M. Zhang, *J. Catal.*, 2021, **399**, 182–191.
8 M. Ji, X. Chi, M. Guo and M. Zhang, *Inorg. Chim. Acta*, 2025, **587**, 122800.
9 X. Xu, J. Xu, N. Lu and M. Zhang, *Langmuir*, 2025, **41**(40), 27537–27546.
10 M. Guo, J. Zhao, S. Han, J. Xu, X. B. Yin and M. Zhang, *Colloids Surf., A*, 2025, 137448.
11 Y. Chen, H. Li, M. Guo, J. Zhao, J. Xu, X. B. Yin and M. Zhang, *Colloids Surf., A*, 2025, 137539.
12 Y. Sun, J. Liu, J. Chen, G. Li, M. Liang and M. Zhang, *Desalination*, 2025, **614**, 119183.
13 B. Mandal, M. Das, M. T. Htay and S. Mukherjee, *Mater. Res. Bull.*, 2019, **109**, 281–290.
14 R. Malik, N. Joshi and V. K. Tomer, *Mater. Adv.*, 2021, **2**(13), 4190–4227.
15 S. Gao and A. C. H. Sue, *Chem*, 2024, **10**(12), 3533–3535.
16 C. Wei, B. Xi, K. Tian, X. Zhang, Q. Man, K. Bao, W. Mao, J. Feng and S. Xiong, *Nano Res.*, 2024, **17**(9), 8145–8154.
17 X. Wei, X. Luo, F. Wang, J. Huang, F. Xiong, W. Zhou and H. Liu, *Adv. Mater. Interfaces*, 2025, e00507.
18 H. S. Khanna, N. A. Eddy, Y. Dang, T. S. Bhosale, S. Shubhashish, S. L. Suib and P. Nandi, *ACS Appl. Energy Mater.*, 2020, **3**(12), 11923–11932.
19 G. S. Day, H. F. Drake, A. Contreras-Ramirez, M. R. Ryder, K. Page and H. C. Zhou, *Cryst. Growth Des.*, 2021, **21**(8), 4249–4258.
20 Z. Shi, C. Shi, H. Shi, B. He, G. Qin, A. Li, J. Zhu and J. Chen, *Particuology*, 2023, **83**, 32–39.
21 J. Li, H. Ren, X. Zou, K. Cai, N. Zhao and G. Zhu, *Chem. Commun.*, 2018, **54**(60), 8335–8338.
22 E. Doustkhah, R. Hassandoost, A. Khataee, R. Luque and M.HN. Assad, *Chem. Soc. Rev.*, 2021, **50**(5), 2927–2953.
23 M. Cheng, P. Lv, X. Zhang, R. Xiong, Z. Guo, Z. Wang, Z. Zhou and M. Zhang, *J. Catal.*, 2021, **399**, 182–191.
24 F. Han, L. Ma, Q. Sun, C. Lei and A. Lu, *Nano Res.*, 2014, **7**(11), 1706–1717.
25 C. Hu, H. Shu, Z. Shen, T. Zhao, P. Liang and X. Chen, *Phys. Chem. Chem. Phys.*, 2018, **20**(25), 17171–17179.
26 F. Yuan, E. Zhang, Z. Liu, K. Yang, Q. Zha and Y. Ni, *ACS Appl. Energy Mater.*, 2021, **4**(11), 12211–12223.
27 S. Yousef and A. Mohamed, *J. Mech. Sci. Technol.*, 2016, **30**(11), 5135–5141.
28 Y. Gu, S. Chen, J. Ren, Y. A. Jia, C. Chen, S. Komarneni, D. Yang and X. Yao, *ACS Nano*, 2018, **12**(1), 245–253.
29 X. Zhang, G. Han and S. Zhu, *Small*, 2024, **20**(3), 2305406.
30 G. Ćirić-Marjanović, I. Pašti, N. Gavrilov and A. Janošević, *Chem. Pap.*, 2013, **67**(8), 781–813.
31 D. P. Dubal, N. R. Chodankar, Z. Caban-Huertas, F. Wolfart, M. Vidotti and R. Holze, *J. Power Sources*, 2016, **308**, 158–165.
32 L. Wu, L. Ji, Y. Xiao, Q. Zhang and Z. He, *Int. J. Hydrogen Energy*, 2024, **64**, 819–829.
33 X. Lu, X. Yang, L. Wang, F. Li, H. Zhang, J. Li and L. Zan, *J. Electroanal. Chem.*, 2023, **931**, 117160.
34 F. Li, N. Mushtaq, T. Su, Y. Cui and J. Huang, *Mater. Today Nano*, 2023, **21**, 100287.
35 G. Li, G. Xie, D. Chen, C. Gong, X. Chen, Q. Zhang, B. Pang, Y. Zhang, C. Li, J. Hu, Y. Chen and L. Yu, *Appl. Surf. Sci.*, 2022, **585**, 152683.
36 B. Cong, X. Li and G. Chen, *Chem. Eng. J.*, 2023, **460**, 141713.
37 G. Raj, R. Nandan, P. Gakhad, K. Kumar, A. K. Singh and K. K. Nanda, *Chem. Eng. J.*, 2025, **503**, 158041.
38 M. Zhang, L. Chen, J. Zheng, W. Li, T. Hayat, N. S. Alharbi, W. Gan and J. Xu, *Dalton Trans.*, 2017, **46**(28), 9172–9179.
39 L. Chen, M. Zhang, X. Yang, W. Li, J. Zheng, W. Gan and J. Xu, *J. Alloys Compd.*, 2017, **695**, 3339–3347.
40 C. Jia, H. Liu, Y. Hu, H. Wu, C. Zhu, Y. Zhang, S. Wang and M. Huang, *ChemistrySelect*, 2021, **6**(25), 6564–6573.
41 H. Li, Z. Jin, N. Lu, J. Pan, J. Xu, X. B. Yin and M. Zhang, *Dalton Trans.*, 2024, **53**(16), 6974–6982.
42 Q. Niu, M. Zhang, L. Liu, J. Zheng, Q. Fang and J. Xu, *CrystEngComm*, 2020, **22**(32), 5302–5309.
43 Q. Niu, M. Zhang, L. Liu, J. Zheng, Q. Fang and J. Xu, *Dalton Trans.*, 2020, **49**(32), 11120–11128.
44 T. Zeng, X. Zhang, H. Niu, Y. Ma, W. Li and Y. Cai, *Appl. Catal., B*, 2013, **134**, 26–33.
45 Y. Wang, H. Zhao, M. Li, J. Fan and G. Zhao, *Appl. Catal., B*, 2014, **147**, 534–545.
46 T. Miao, J. Zheng, J. Wang, J. Xu, N. S. Alharbi and M. Zhang, *Dalton Trans.*, 2018, **47**(46), 16578–16586.
47 J. Zheng, J. Wang, D. Song, J. Xu and M. Zhang, *ACS Appl. Nano Mater.*, 2020, **3**(4), 3449–3458.
48 J. Wang, M. Zhang, T. Miao, Y. Ling, Q. Wen, J. Zheng, J. Xu, T. Hayat and N. S. Alharbi, *Inorg. Chem. Front.*, 2018, **5**(4), 844–852.
49 Y. Liu, B. Zhang, Y. Yang, Z. Chang, Z. Wen and Y. Wu, *J. Mater. Chem. A*, 2013, **1**(43), 13582–13587.
50 A. Jayaraman and H. A. Klok, *ACS Polym. Au*, 2022, **2**(6), 387–391.
51 L. Li, Z. Wei, J. Liang, J. Ma and S. Huang, *Results Chem.*, 2021, **3**, 100205.
52 S. Srinithi, V. Balakumar and S. M. Chen, *Chemosphere*, 2022, **291**, 132977.

53 K. Beamsley, N. Hosono and T. Uemura, *Nat. Commun.*, 2025, **16**(1), 6984.
54 J. R. Xavier, *J. Adhes. Sci. Technol.*, 2020, **34**(2), 115–134.
55 S. K. Fanourakis, J. Peña-Bahamonde and D. F. Rodrigues, *Environ. Sci.:Nano*, 2020, **7**(12), 3794–3804.
56 A. Pugazhendhi, S. Vasantharaj, S. Sathiyavimal, R. K. Raja, I. Karuppusamy and M. Narayanan, *Surf. Coat. Technol.*, 2021, **425**, 127739.
57 Q. Zeng, J. Chen, F. Gao, X. Tu, Y. Qian, Y. Yu and L. Lu, *Synth. Met.*, 2021, **271**, 116620.
58 L. Wang, Y. Xu, X. Tan, S. Tapas and J. Zhang, *RSC Adv.*, 2017, **7**(58), 36201–36207.
59 O. Ejeromedoghene and B. Kpomah, *Chem. Afr.*, 2024, **7**(5), 2857–2865.
60 T. Hu, B. Xue, F. Meng, L. Ma, Y. Du, S. Yu, R. Ye, H. Li, Q. Zhang, L. Gu, Z. Zhou, R. Liang and C. Tan, *Adv. Healthcare Mater.*, 2023, **12**(11), 2202911.
61 D. Vikraman, H. Liu, S. Hussain, K. Karuppasamy, H. K. Youi, J. Jung, J. Kang and H. S. Kim, *Appl. Surf. Sci.*, 2021, **543**, 148863.
62 A. H. Alshammari, M. Alshammari, M. Ibrahim, K. Alshammari and T. A. M. Taha, *Opt. Laser Technol.*, 2024, **168**, 109833.
63 L. Song, J. Ren, J. Zhao, H. Ding and Y. Zhang, *Sep. Purif. Technol.*, 2025, 135093.
64 J. Wang, M. Zhang, T. Miao, Y. Ling, Q. Wen, J. Zheng, J. Xu and T. Hayat, *Inorg. Chem. Front.*, 2018, **5**(4), 844–852.
65 M. J. Zhao, E. M. Li, N. Deng, Y. Hu, C. X. Li, B. Li, F. Li, Z. G. Guo and J. B. He, *Renewable Energy*, 2022, **191**, 370–379.
66 J. Feng, Y. He, Y. Liu, Y. Du and D. Li, *Chem. Soc. Rev.*, 2015, **44**(15), 5291–5319.
67 M. Israr, S. Ali, J. Zhang, Y. Zeng, M. Humayun, H. Yu, X. Chen, C. Chen and Y. Li, *Small*, 2025, **21**(20), 2500828.
68 V. S. Smitha, A. Swargy, M. Digilarani, T. Vimala and T. R. Resmi, *New J. Chem.*, 2024, **48**(37), 16202–16214.
69 M. Sharif and S. Tavakoli, *Polym. Bull.*, 2024, **81**(13), 11481–11498.
70 A. Ćirić, S. Stojadinović and M. D. Dramićanin, *J. Alloys Compd.*, 2022, **900**, 163544.
71 J. Wang, M. Zhang, J. Xu, J. Zheng, T. Hayat and N. S. Alharbi, *Dalton Trans.*, 2018, **47**(8), 2791–2798.
72 F. Han, L. Ma, Q. Sun, C. Lei and A. Lu, *Nano Res.*, 2014, **7**(11), 1706–1717.
73 X. He, M. Zhang, Z. Jin, J. Zheng, J. Xu and X. B. Yin, *Dalton Trans.*, 2022, **51**(43), 16681–16687.
74 L. Yang, J. Zheng, J. Xu, B. Zhang and M. Zhang, *CrystEngComm*, 2021, **23**(42), 7517–7524.
75 Z. Yin, X. Liu and S. Chen, *Mater. Today Nano*, 2022, **17**, 100156.
76 Y. Feng and H. Liu, *Appl. Surf. Sci.*, 2021, **538**, 147992.
77 J. Joyner, E. F. Oliveira, H. Yamaguchi, K. Kato and S. Vinod, *ACS Appl. Mater. Interfaces*, 2020, **12**(11), 12629–12638.
78 E. B. Kim, M. S. Akhtar and S. Ameen, *Chemosphere*, 2024, **369**, 143796.
79 M. Adhikari, D. Saha, D. Chattopadhyay and M. Pal, *ACS Appl. Eng. Mater.*, 2025, **3**(5), 1302–1314.
80 L. Tang, B. Zhang, T. Peng, Z. He, C. Yan, J. Mao, K. Dai, X. Wu and J. Zheng, *Nano Energy*, 2021, **90**, 106568.
81 L. Chen, Y. Dong, H. Jiang, Y. Hu and C. Li, *Chem. Eng. Sci.*, 2022, **261**, 117953.
82 H. Wang, L. Guo, J. Pan, J. Xu, X. B. Yin and M. Zhang, *Dalton Trans.*, 2024, **53**(31), 12973–12984.
83 M. Huang, X. R. Shi, X. He, X. Zhang, F. Cao, P. Wang, C. Sun, S. Xu and M. Zhang, *Electrochim. Acta*, 2022, **427**, 140884.
84 M. Huang, H. Yao, F. Cao, P. Wang, X. R. Shi, M. Zhang and S. Xu, *J. Colloid Interface Sci.*, 2024, **676**, 471–484.
85 S. He, Y. Zhang, J. Ren, B. Wang, Z. Zhang and M. Zhang, *Colloids Surf., A*, 2020, **600**, 124900.
86 S. R. Ali and M. De, *ACS Appl. Nano Mater.*, 2021, **4**(11), 12682–12689.
87 J. Chen, Y. Sun, M. Zhang, J. Zhao, L. Song, L. Yan and G. Li, *Desalination*, 2024, **590**, 117981.
88 R. Naz, W. Abbas, Q. Liu, S. Shafi, S. Gull, S. Khan, T. Rasheed, G. Song and J. Gu, *J. Alloys Compd.*, 2023, **951**, 169944.
89 J. Xu, G. Shao, X. Tang and S. Liu, *Nat. Commun.*, 2022, **13**(1), 2193.
90 Y. Long, X. Wang, W. Tan, B. Li, J. Li, W. Deng, X. Li, W. Guo and J. Yin, *Nano Lett.*, 2024, **24**(25), 7572–7577.
91 Y. Tan, H. Jiang, B. Wang and X. Zhang, *New J. Chem.*, 2021, **45**(41), 19593–19604.
92 M. Sreeramareddygari, M. Somasundrum and W. Surareungchai, *New J. Chem.*, 2020, **44**(15), 5809–5818.
93 W. Zhang, P. Zhang, Z. Su and G. Wei, *Nanoscale*, 2015, **7**(44), 18364–18378.
94 Q. Chen, F. Xie, G. Wang, K. Ge, H. Ren, M. Yan, Q. Wang and H. Bi, *Ionics*, 2021, **27**(9), 4083–4096.
95 J. Ma, H. Ren, Z. Liu, J. Zhou, Y. Wang, B. Hu, Y. Liu, L. B. Kong and T. Zhang, *Compos. Sci. Technol.*, 2020, **198**, 108239.
96 Z. Li, M. Zhang, L. Liu, J. Zheng, H. Alsulami, M. A. Kutbi and J. Xu, *Colloids Surf., A*, 2020, **605**, 125347.
97 Y. Ling, T. Cao, L. Liu, J. Xu, J. Zheng, J. Li and M. Zhang, *J. Mater. Chem. B*, 2020, **8**(34), 7801–7811.
98 H. Peng, J. Zheng, B. Zhang, J. Xu and M. Zhang, *Dalton Trans.*, 2021, **50**(42), 15380–15388.
99 Z. Lu, N. Lu, Y. Xiao, Y. Zhang, Z. Tang and M. Zhang, *ACS Appl. Mater. Interfaces*, 2022, **14**(9), 11156–11166.
100 Y. Liu, S. Zhang, Y. He, C. Chen and C. Zhang, *Coatings*, 2021, **11**(2), 178.
101 Y. Chen, H. Li, J. Xu, X. B. Yin and M. Zhang, *Langmuir*, 2025, **41**(21), 13645–13654.
102 C. Li, Z. Wang, Y. Jin, Z. Li and J. P. Jeon, *Angew. Chem.*, 2025, **137**(14), e202500336.
103 P. Najmi, N. Keshmiri, M. Ramezanzadeh, B. Ramezanzadeh and M. Arjmand, *ACS Appl. Mater. Interfaces*, 2022, **14**(48), 54141–54156.
104 M. Guo, Z. Jin, J. Pan, J. Xu, L. Guo, X. B. Yin, N. Lu and M. Zhang, *Inorg. Chem.*, 2024, **63**(39), 18263–18275.

